Journal of Alloys and Compounds 382 (2004) 29–38

Journal of ALLOYS AND COMPOUNDS

www.elsevier.com/locate/jallcom

Surfaces and interfaces characterization by neutron reflectometry

F. Ott*, F. Cousin, A. Menelle

Laboratoire Leon Brillouin CEA/CNRS UMR12, bat 563, Centre d'Etudes de Saclay, 91191 Gif sur Yvette Cedex, France

Received 22 September 2003; received in revised form 15 February 2004; accepted 20 March 2004

Abstract

Neutron reflectivity allows to characterize surfaces and interfaces of ultra-thin film layered systems down to a nanometric scale (∼2 nm). It is a powerful tool for the study of magnetic and polymer thin film structures. The neutron magnetic interaction is of the same order as the nuclear interaction and makes polarised neutron reflectivity a very sensitive tool for probing magnetic multilayers. It allows the determination of magnetic ordering and coupling in artificial magnetic multilayers (either metallic/semi-conducting or oxides). Examples of studies in the field of giant magneto resistive (GMR) sensors used in hard drive and tape read heads are given. The search for efficient spin-injection materials which could be used in spin electronics is also a growing field of activity. Several material candidates are presently evaluated. Recent studies on such materials are presented: oxide materials (Fe_2O_3–Fe_3O_4) epitaxial thin films; multilayer systems involving semiconducting materials ($(Fe/Si)_n$–(GaMnAs/GaAs)). Besides the high sensitivity of neutrons to magnetism, the possibility of isotopic labelling (H/D substitution) offers a way to probe polymer and protein thin film structures with great details: polymer interdiffusion or polymer grafting can be studied at the substrate–polymer or liquid–polymer interfaces. A model study of polymer grafting is presented.

Keywords: Magnetic films and multilayers; Polymers; Elastomers and plastics; Surfaces and interfaces; Neutron diffraction; Magnetic measurements

1. Introduction

Neutron reflectometry (NR) is a relatively new technique [1,2]. It has been extensively used for solving soft matter problems like polymer mixing [3,4] or the layout of large molecules at the surface of liquids [5,6]. The advantage of neutrons for polymer studies is their small absorption compared to X-rays and the large contrast between ^1H and ^2H which allows selective labelling by deuteration. In the late 1980s, a new field of application of neutron reflectometry emerged. Following the discovery of giant magneto-resistance in anti-ferromagnetically coupled multilayered films [7] and new phenomena in ultra-thin films, there has been an interest in the precise measurement of the magnetic moment directions in each layer and at the interface between layers. Owing to the large magnetic coupling between the neutron and the magnetic moment, neutron reflectometry is a powerful tool for obtaining information about these magnetic configurations. In this short review, we will focus on specular reflectivity. In the first part, we will present the technique of neutron reflectivity. In the second part, the use of neutrons for the study of polymers is presented. In the last part, we focus on recent examples of studies of materials by polarised neutron reflectivity (PNR).

2. Neutron reflectivity (NR) principles

Neutrons can be reflected on surfaces in the same way as X-rays or electrons [8]. All the formalisms developed for X-ray reflectivity can be almost directly transposed for neutron reflectivity [9]. The neutron–matter interaction is a direct interaction between the neutron and the nucleus and not with the electronic cloud as for X-rays. The neutron–nucleus interaction is very short range and depends not only on the position of the element in the periodic table (Z number) but also on the isotope of the considered element (A number). This property is widely used for the study of colloids and polymers, where hydrogen (^1H) can be replaced by deuterium (^2H) to do a so-called isotopic labelling. The amplitude of the neutron–matter interaction

* Corresponding author. Tel.: +33-1-69-08-61-21/65-16; fax: +33-1-69-08-82-61.
E-mail address: fott@cea.fr (F. Ott).
URL: http://www-llb.cea.fr/prism/PRISM.html.

0925-8388/$ – see front matter © 2004 Published by Elsevier B.V.
doi:10.1016/j.jallcom.2004.05.046

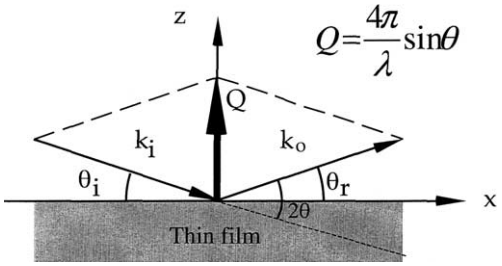

Fig. 1. Geometry of a specular reflectivity experiment. The scattering wave-vector **Q** is perpendicular to the plane of the thin film.

is tabulated and varies randomly from one atom to the other [10]. It is usually repulsive but can be attractive in a few cases (^{1}H, Ti, V, Mn). The absorption of neutron by matter is weak and can usually be neglected for reflectivity measurements (except for B, Gd, Li, Cd).

In a reflectivity geometry (see Fig. 1), the incidence angle θ_i on the surface is small (typically ranging from 0.5 to 5°). The reflection angle θ_r is the same as the incidence angle θ_i. As a consequence, the scattering wave-vector **Q** is perpendicular to the surface. The typical neutron wavelengths are in the range of 2–20 Å. Thus, the range of accessible scattering wave-vector $\mathbf{Q}=k_o-k_i$, is in the range of 0.05–3 nm^{-1}. This corresponds in the real space to typical length-scales between 2 and 100 nm. NR is a technique adapted for the study of thin films but does not probe structures at the atomic level. In a reflectivity geometry, it is thus possible to do the "optical approximation" [9] and to model the neutron interaction with the material as a continuous potential (the details of the atomic structure are smoothed out). The interaction potential V with a material is given by:

$$V = \frac{h^2}{2\pi m}\rho \text{ with } \rho = \sum_i N_i b_i \tag{1}$$

where h is the Planck constant and m the neutron mass; ρ is called the "scattering length density" (SLD) and is the sum of the atomic density of the nuclei in your material N_i, multiplied by their individual nuclear scattering lengths b_i. Tables of the different scattering lengths can be found in [10–12].

In the case of a magnetic system, the interaction between the neutron spin and the material magnetisation is of the form $V = -\vec{\mu}\cdot\vec{B}$, where $\vec{\mu}$ is the neutron magnetic moment and $\vec{B}$ is the magnetic induction inside the thin film. One must note, that neutrons are only sensitive to the magnetic induction and thus cannot distinguish between spin and orbital moment.

In the reflectivity geometry, the equivalent of a neutron "optical index" can be derived from the Schrödinger equation [9]. Neglecting absorption, the value of this optical index is given by the following expression:

$$n \approx 1 - \delta \pm \delta_M = 1 - \frac{\lambda^2}{2\pi}\rho \pm \frac{m\lambda^2}{h^2}\mu B \tag{2}$$

Table 1
The neutron, nuclear and magnetic optical indexes $n = 1 - \delta \pm \delta_M$ for common materials at $\lambda = 0.4$ nm

Element	δ (10^{-6})	δ_M (10^{-6})	σ_a (barns)
Fe	20.45	11.7	2.56
Co	5.7	10.3	37.2
Ni	24	3.7	4.49
Gd	5.0	14.5	49,700
Si	5.3	–	0.17
Ti	−5	–	6.1
Al	6.11	–	0.23
SiO_2	10.1	–	
H_2O	−1.43	–	
D_2O	16.2	–	
H-polystyrene	3.6	–	
D-polystyrene	16.5	–	

where δ is the nuclear contribution to the optical index, and $\delta_M$is the magnetic contribution to the optical index, the sign of the magnetic contribution depends on the relative orientation of the neutron spin with respect to the magnetisation (parallel or anti-parallel). Table 1 gives examples of optical indexes for some typical materials. One should notice that the magnetic optical index is of the same order of magnitude as the nuclear optical index.

In a reflectivity measurement, the most important assumption made is that the system is invariant in translation in the thin film plane, that is, there are no inhomogeneities along the film surface. Thus, the interaction potential V is assumed to be only a function of the depth z in the multilayer system: $V(z)$ and $n(z)$. In the Born approximation, the scattering amplitude is given by:

$$\frac{h^2}{2\pi m^2} f(k_i, k_o) = -\int_\Omega dv\, e^{-ik_o z} V(z) e^{+ik_i z} = -\int_\Omega dv\, V(z) e^{-iQz} = -\tilde{V}(Q) \tag{3}$$

where, $\mathbf{Q}=k_i-k_o$ is the scattering wave-vector (see Fig. 1) and $\tilde{V}(\boldsymbol{Q})$ is the Fourier transform (along Oz) of the interaction potential. In the first approximation, reflectivity measures the Fourier transform of the optical index profile $n(z)$.

However, at low incidence angles, there is total reflection up to a critical wave-vector $\boldsymbol{Q}_c = 4\sqrt{\pi\rho}$ (see Fig. 2), and thus, the Born approximation is not valid at small scattering wave-vectors. The Born approximation can be applied only above a scattering wave-vector of $3\mathbf{Q}_c$. Below this limit, one must solve the Schrödinger equation and perform a full dynamical calculation [9]. Fig. 2a presents the situation of the reflection of a neutron beam on a semi-infinite medium: above the critical wave-vector of total reflection, the reflected intensity decreases as $1/\mathbf{Q}^4$. The reflectivity of a multilayer Si/Cu/Cr is also presented. Modulations of the reflected intensities are observed which correspond to constructive and destructive interferences of the neutron waves scattered by the different interfaces of the multilayer system. These oscil-

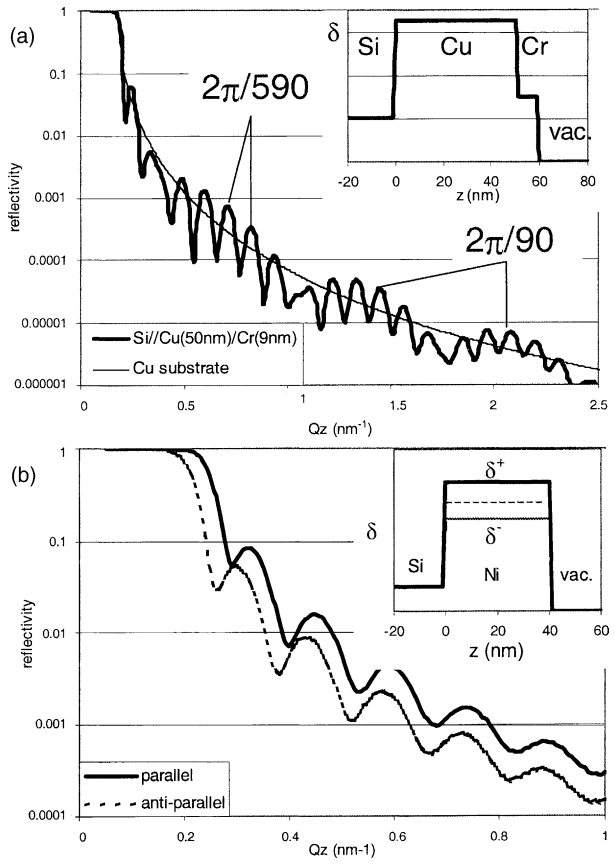

Fig. 2. (a) Reflectivity on a semi infinite medium (copper substrate) and on a multilayer system Si//Cu (50 nm)/Cr (9 nm). The short range oscillations are characteristic of the total thickness of the layer (59 nm); the long range modulations are characteristic of the thin Cr cap layer (9 nm), (inset). The optical index profile as a function of the depth in the film. (b) Reflectivity on a magnetic thin film Si//Ni (40 nm). The reflectivity depends on the relative orientation of the neutron spin with respect to the magnetic field (inset) the optical index profile for the two neutron polarisations (parallel and anti-parallel).

lations are called Kiessig fringes. Their pattern is characteristic of the multilayer system. Fig. 2b presents the situation of a magnetic thin film on a substrate. In this case, the optical index depends on the relative orientation of the neutron spin with respect to the thin film magnetisation. The measured reflectivity is very different for neutron incident with a spin parallel to the magnetisation (optical index δ^+) and for neutrons incident with a spin anti-parallel to the magnetisation (optical index δ^-). The insets of the Fig. 2 show the optical index profile along the multilayer depth (Oz).

The measure of the reflectivity as a function of **Q**, probes the profile of optical index $n(z)$ along the normal (Oz) to the thin film system. The use of numerical models then allows to reconstruct the thickness of the different layers of the system as well as their individual SLD which is characteristic of their chemical composition. More detailed models also allow to measure inter-diffusion and roughness at interfaces. In the case of magnetic systems, NR allows to measure the absolute magnetisation of the different layers.

3. Real experiments

3.1. Reflectivity spectrometers

A reflectivity experiment consists in sending a neutron beam on a surface and varying the scattering wave-vector. This can be performed in two ways in a neutron experiment. The first possibility is to use a fixed wavelength (defined by a monochromating crystal) and perform a standard θ–2θ scan. The second possibility is to work at a fixed incidence angle and to scan the incident wavelength. Cold neutrons have a typical slow travel speed of the order of 1000 m/s which depends on the wavelength: $v = h/m\lambda$. Thus, if one sends a neutron pulse (defined with a chopper and of typical duration 0.2 ms), a spatial spread of the neutrons of different wavelengths takes place between the chopper and the detection systems. The neutron wavelength can then simply be measured by the travel time between the chopper and the detector. This technique is called time-of-flight (ToF). Fig. 3 shows the typical layout of a ToF reflectometer. In practice, the wavelength spectrum (typ: 2–20 Å) is not wide enough to cover a very large **Q**-range in the reciprocal space. Thus, usually two or more different incidence angles are used to cover a wider **Q**-range. One advantage of a ToF set-up is that it is very easy to change the resolution by changing the chopper and slits parameters. Another advantage is that the sample does not need to be moved during an experiment and thus, it is easier to measure free liquid surfaces. A review of existing spectrometers can be found in [13,14].

3.2. Real systems

3.2.1. Sample sizes–measurements time

One has to keep in mind that most existing reflectometers are optimised to perform experiments on samples which have a surface of the order of 10 cm^2. In the case of optimised reflectometers with focussing systems (such as PRISM at the LLB), it is possible to perform experiments on samples which have a size of the order of 1 cm^2. These limitations in size imply that the studied samples need to have a very good homogeneity over a very large surface: the thickness of the layers need to be homogeneous and the substrate needs to be flat over the whole sample surface. If this is not the case, only averages over the sample surface will be measured and the information that can be obtained about the sample will be limited. The reflectivity signal drops very quickly with the scattering wave-vector value. For a perfect interface, at large

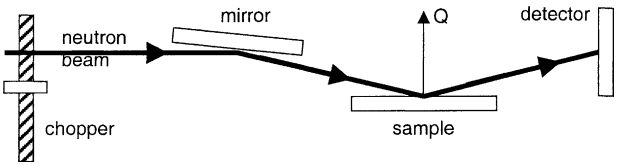

Fig. 3. Schematic of a time of flight reflectometer: a chopper defines neutron pulses; the neutron wavelength is defined by the travel time between the chopper and the detector. The sample position is fixed.

Q values, the reflectivity is proportional to $1/\mathbf{Q}^4$. **Q** values of the order of 2–3 nm^{-1} typically correspond to reflectivity of the order to 10^{-6} and require measurements of the order of 2–6 h.

3.3. Sample environment

The absorption of neutrons is negligible in most materials. The typical penetration depth for materials such as silicon or aluminium is of the order of 50 mm (depending of the wavelength). This makes it easy to set-up complex sample environments on neutron spectrometers. The available ancillary equipments includes: cryomagnets (temperature range: 1.6–300 K; magnetic field range: 0–7 T), furnaces (temperature up to 800 °C); closed liquid cells (made of quartz or silicon).

3.4. Analysis of experimental data

Reflectivity curves cannot be directly inverted. It is often possible to build a family of SLD profiles which give the same reflectivity curve. This is due to the fact that only the intensity and not the phase of the reflectivity are measured [15]. The analysis of experimental data is done by adjusting the different parameters involved in the problem until a good least square fit is obtained. The main source of uncertainty on the result is in general due to the lack of intensity at high **Q** and the roughness of the sample. In the case of magnetic systems, the composition and the thickness of the different layers is usually rather well defined. One needs to fit the roughness, the thicknesses and the magnetic moments magnitude. It is in general very useful to have some external information coming from X-rays reflectometry, ellipsometry and magnetic hysteresis measurements.

4. Example of non-polarised reflectivity

4.1. Polymers-isotopic labelling

The substitution of hydrogen by deuterium in organic materials allows to strongly change the neutron optical index of the material (see Table 1) without changing its physical or chemical properties. A very interesting possibility offered by neutron scattering is to do selective labelling by deuteration [16,17]. Such labelling is used in two ways: (i) it allows to measure the conformation of polymeric chains at the interface in good solvent by using hydrogenated polymers in deuterated solvents (for example, adsorption profiles of polymers at interfaces have been measured by neutron reflectivity [18–21]). (ii) It allows to determine the structure of 'complex' systems involving two polymers by mixing hydrogenated and deuterated polymers. This can be achieved with deuterated and hydrogenated chains of the same polymer (to study the interdiffusion of chains at the interface of two molten polymers for example [22]) or of different polymers (multilayers of polyelectrolyte of opposite charges for example [23]). Combining these two advantages to determine the structure of a mixture of two different polymers in good solvent is possible by using the variation contrast method: measurements are performed in successive mixtures of hydrogenated and deuterated solvent that either match the neutron optical index of the first polymer, or match the neutron optical index of the second one. It allows to resolve the whole structure of the system [24].

To illustrate these two aspects we shall present a recent study on the conformation of dense grafted brushes of polystyrene (PS) on silicon [25]. Such macromolecular architecture are designed to answer the technological demand of controlled and reproducible thin polymers films. It is based on recent, grafting from techniques that allow to graft polymers onto a surface in an efficient way. Classically, the most common method for polymer grafting is the "grafting onto" method, where end functionalised polymers react with appropriate surface sites. In this more promising "grafting from" method, the chains grow in situ from preformed surface-grafted initiators [26]. This latter approach is thus, a suitable way for building high-density polymer brushes because it is not limited by polymer diffusion. It also allows a fine control of the polymer layer. This strategy has been applied by Devaux et al. [25] to realize grafted brushes of PS on silicon which have been studied by neutron reflectivity.

In order to test the homogeneity of the chains growth during the polymerisation process, a specific chain designed for neutron reflectivity measurement has been fabricated with a two-steps process: the first part of the chains has been grown using deuterated monomers and the second part using hydrogenated monomers (Fig. 4a). Chemically, the polymer chains behave as a single physical unit. However, NR allows to easily distinguish between the two parts of the chains as shown in Fig. 4c that presents the reflectivity of the polymer layer at the polymer–air interface: Kiessig fringes arise from the deuterated layer, the hydrogenated layer and the whole layer. It allows a very accurate determination of the width of the interface thickness between the deuterated and the hydrogenated parts of the polymers: if the width is null we would get large oscillations from the deuterated layer and if it is too large we only get small oscillations from the whole layer as other oscillations vanishes (Fig. 4c presents the simulated profiles of Fig. 4b). Best fit shows that the interface width is limited to 2.5 nm for a brush of thickness 43 nm. This proves that this "grafting from" technique allows to built very well ordered polymer brushes and that the growth of the brushes is very homogeneous.

The swelling capacities of the PS brushes in good solvent have been measured in the second part of the study: an hydrogenated brush of a dry thickness of 220 Å was placed into a good solvent of PS (deuterated toluene). As it has been said before, the absorption of neutrons is very low and this allows to use the silicon substrate as the incident medium (even though the travel in the silicon is larger than 50 mm) (see Fig. 5a). Fig. 5b presents the monomeric concentra-

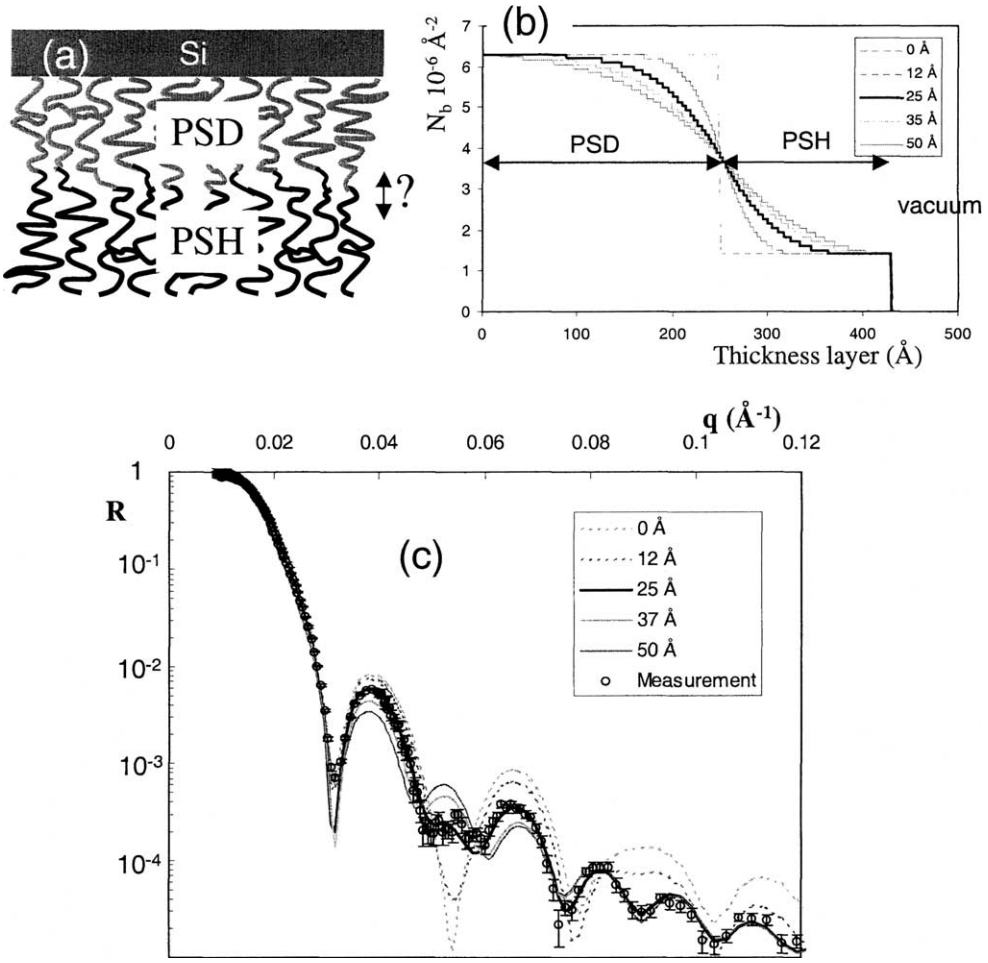

Fig. 4. Reflectivity on a polymer grown using a "grafting from" method: (a) a polymer layer grafted on a silicon substrate, half of the layer is hydrogenated, the second half of the layer is deuterated; (b) optical index along the thickness of the layer assuming different interface thickness (the profile is assumed to vary as an erf function); (c) reflectivity of the system and theoretical curves for the different thickness of the interfacial layer (zone separating the H- and D-polymer layers). The best agreement is obtained for an interfacial layer of thickness 25 Å [25].

tion profile as a function of the depth deduced from the fit of experimental reflected curves. It shows that the swelling of the layer is limited. The volume fraction ϕ of the polymer remains as high as 0.8 of the density of the dry polymer showing that the solvent hardly penetrates the layer. At the polymer–solvent interface, one can observe a parabolic variation of the polymer density. Three fitting methods have been tested and provide very similar results. The detailed information about the very top of the polymer layer is limited because the **Q**-range of the measurement was limited. The maximal stretch of the layer can nevertheless be evaluated as it roughly corresponds to the maximal extension of the profile (300 Å). It shows that the chains were already strongly stretched in their dry state (∼0.7) as the layer width was 220 Å. Such initial strong stretching is due to a very high density of grafting of polymeric chains that explains the unusual low swelling capacities of the brushes. This example illustrates some of the unique possibilities offered by neutron reflectivity for the study of solid–liquid interfaces.

4.2. Other possibilities

Neutron reflectivity may also be used to probe oxide layers, since the neutron optical index of oxides are usually very different from non oxidized materials (e.g. $\delta_{Si} = 5.3 \times 10^{-6}$ and $\delta_{SiO_2} = 10.1 \times 10^{-6}$). For example, the preparation of SiO_2 oxide films on silicon substrate by three different methods (thermal, chemical and electrochemical oxidation) have been compared by Bertagna et al. [27]. NR may also be useful in the case of some specific materials such as boron (e.g. study of borophosphosilicate glass on Si [28]) or titanium (such as TiO_2 as used in glazing [29]). Boron is strongly absorbing neutrons and titanium has a negative scattering length.

Biology is a field where the use of NR has been growing these last years, mainly for the study of biophysical problems at solid-liquid interfaces. For the readers interested in this field, they shall refer to the recent review of Fragneto-Cusani [30].

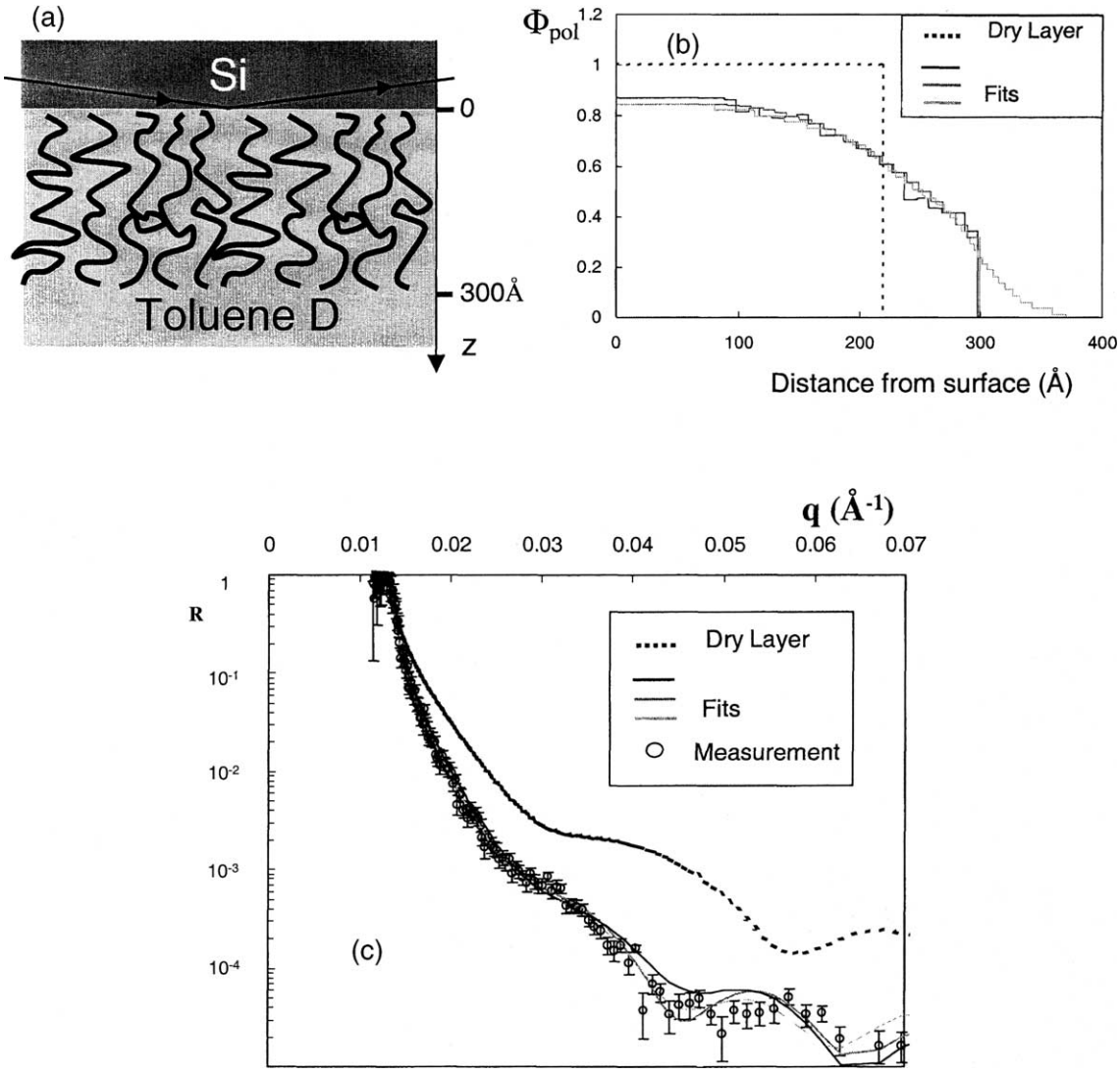

Fig. 5. PS layer in a good solvent (toluene): (a) the measurement set-up, with the neutron beam incident on the system through the silicon substrate; (b) fit of the polymer density profile ϕ in deuterated toluene (three fitting methods of the NR data have been tested and give very similar results). The polymer density ϕ is normalised to 1 for the dry layer, (c) reflectivity measurement and numerical modelling curves [25].

5. Polarised neutron reflectivity (PNR)

Beside the study of polymer systems, the second field in which NR has proved to be a powerful tool is the study of magnetic thin films and multilayers: exchange coupling in superlattices [31,32], exchange bias coupling between ferro- and anti-ferromagnetic layers [33–39], exchange spring effects between soft and hard magnetic layers [40,41], ultra-thin films [42–44]. The neutron has a spin which makes it a very sensitive probe to the magnetisation of thin films. The magnetic scattering length is of the same order of magnitude as the nuclear scattering length (see Table 1). The detailed theoretical treatment of the PNR can be found in [1,9,45–47]. In practice one can say that PNR allows to obtain information on the amplitude of the magnetisation of the different layers of a system in the same way as can be done in the non polarised case. One should also note that PNR is sensitive to the induction in the thin films: no difference is made between the spin (S) and orbital (L) magnetic moments. In a PNR experiment, an extra parameter can be controlled which is the applied magnetic field on the sample. PNR uses the fact that neutrons can be polarised in a way similar to light. In the following we shall refer to “up” (respectively, “down”) neutrons as neutrons with their spins parallel (respectively, anti-parallel) to the applied field. In a PNR experiment, it is thus possible to measure four cross-sections: two non spin–flip cross sections, R^{++}(respectively, R^{--}), corresponding to the number of incoming “up” (respectively, “down”) neutrons reflected with an “up” (respectively, “down”) polarisation; two spin–flip cross-sections, $R^{+-} = R^{-+}$, corresponding to the number of neutrons experiencing a spin–flip during the reflection on the sample. In the first approximation, the non-spin–flip cross sections mainly probe the components of the magneti-

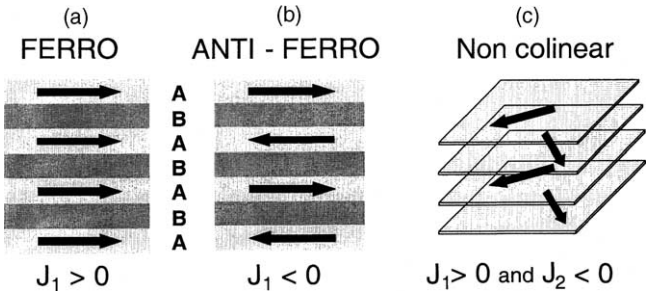

Fig. 6. Schematic of different magnetic configurations which can be observed in a magnetic super-lattice (Ferro/Spacer)$_n$, where the Ferromagnetic layers and the Spacer layers have thickness of the order of a few nanometres (1–4 nm). Depending on the exchange coupling between the layers, one can observe either: (a) a ferromagnetic ordering; (b) an anti-ferromagnetic ordering or (c) a magnetic structure with perpendicular magnetic moments.

sation which are parallel to the applied field; the spin–flip cross sections are sensitive to the component of the magnetisation perpendicular to the applied field. Combining these information it is possible to reconstruct the magnetisation direction. In the following, we shall restrict ourselves to two examples illustrating some of the possibilities offered by PNR: super-lattices and PNR magnetometry of complex multilayers. For other examples, the interested reader may also refer to the following recent reviews on PNR [48–50].

5.1. Superlattices

A large amount of results have been obtained by PNR on super-lattices during the 90′ [51–55]. A super-lattice consists of a periodic repetition (n times) of a bilayer system (A/B)$_n$ (see Fig. 6). If the material A is magnetic, then depending on the thickness of the intermediate layer B (from 0.5 to 3 nm) and the type of the B material, (Cr, Mn, Cu, ...) a magnetic coupling can be mediated through this non magnetic B layer. The coupling energy can be described by using an energy of the form:

$$E_{\text{coupling}} = -J_1 \vec{S}_1 \cdot \vec{S}_2 - J_2 (\vec{S}_1 \cdot \vec{S}_2)^2$$

Depending on the sign and magnitude of the coupling constants J_1 and J_2, a variety of magnetic orderings can be observed (see Fig. 6). Usually the coupling constant oscillates between positive and negative values as a function of the thickness of the B spacer, thus the magnetic order between the A layers changes from ferromagnetic to anti-ferromagnetic. In some structures it is even possible to observe non-collinear coupling between the different magnetic layers. Fig. 7 shows an example of PNR on a system (Fe (2.5 nm)/Si (1.2 nm))$_n$ [44]. The reflectivity was measured at 20 K in a planar field of 20 mT. At the position $\mathbf{Q} = 0.17\,\text{Å}^{-1}$, the peak is indicative of the period of the super-lattice defined by the thickness 3.7 nm of a (Fe (2.5)/Si (1.2)) bilayer. It corresponds to the (0 0 1) peak of the super-lattice. A magnetic contrast between the UP and DO reflectivities exists corresponding to a net magnetisation component along the applied field. At the position $\mathbf{Q} = 0.085\,\text{Å}^{-1}$, that is (0 0 1/2), a strong diffraction peak is observed. It indicates an anti-ferromagnetic component. But the existence of a very strong spin–flip peak at (0 0 1/2) indicates that a non-collinear magnetic order has set-up in the structure and that the arrangement of the magnetic moments in the structure resembles the one shown in Fig. 6c. Numerical modelling suggests that the Fe layers are arranged so that the magnetisations of alternating Fe layers make an angle of 30° with respect to the applied magnetic field. The magnetic moment of the iron layer is however reduced to 1.4μ_B/Fe atom because of the Si interdiffusion and of the fact that the Fe layers are very thin. PNR also offers the possibility to measure very small magnetic moments in multilayers such as (GaAs/GaMnAs)$_n$. Magnetization as small as 27 kA/m (0.03 T) can be determined [54].

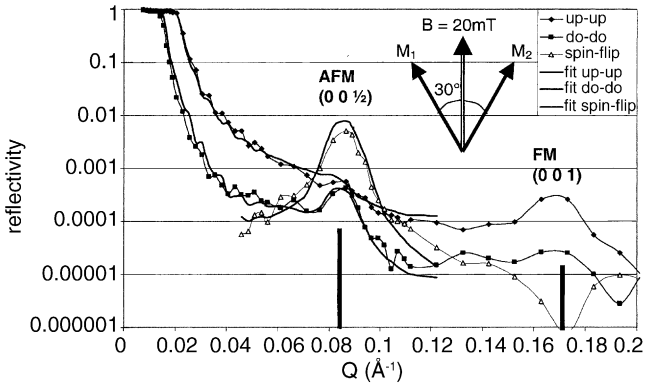

Fig. 7. PNR measurement on a super-lattice involving semi-conducting materials: GaAs//(Fe (2.4 nm)/Si (1.2 nm))$_{20}$ at 7 K under an in-plane magnetic field of 20 mT. The strong spin–flip (0 0 1/2) diffraction peak is indicative of a complex non-collinear magnetic arrangement. The vertical bars indicate the position of the expected super-lattice peaks. The modelling suggests that the Fe layers are arranged so that the magnetisations of alternating layers make an angle of 30° with respect to the applied magnetic field. The magnetic moment of the iron layer is, however, reduced to 1.4μ_B/Fe atom because of the Si interdiffusion and of the fact that the Fe layers are very thin.

5.2. PNR magnetometry

The optimisation of multilayer stacks for magnetic sensors (see Fig. 8a) benefits from the precise knowledge of the behaviour of the different magnetic layers as a function of the applied field. We show here how PNR allows to determine with a high precision, the thickness and magnetic moment configuration and reveals the mechanism of reversal of the "free" soft magnetic layer. The studied GMR spin valve has a rather standard composition: SiO_2/Ta (5)/NiFe (3.7)/CoFe (1.2)/Cu (2.4)/CoFe (2.4)/MnPt (35)/Ta (10). The free layer (NiFe (3.7)/CoFe (1.2)) can rotate in a field of several Oe while the hard layer (CoFe (2.4)/MnPt (35)) is blocked for fields larger than 1 T. The GMR is fabricated with an easy axis of the free layer perpendicular to the magnetisation of the pinned layer. Fig. 8b shows SQUID mea-

surements on the GMR. 1/*f* noise in this optimised GMR sensors is lower than in previous works. The reason for this good behaviour is the absence of domain formation during the magnetisation reversal process of the free layer. In the presence of domains, 1/*f* noise could be several orders of magnitude larger. In order to follow the magnetic configuration as a function of the magnetic field, a first measurement has been performed in a magnetic saturating field of 1 T (see Fig. 8c). Spin–flip reflectivity is then very low due to the absence of non-collinear magnetic moments. The magnetic configuration was then followed as a function of the applied magnetic field for a small set of angles as a function of the applied magnetic field (see Fig. 8c insert). Then, using the parameters deduced from the saturated state, these reflectivities have been adjusted by varying a single parameter: the magnetic direction of the free layer. It appears during the fit that a homogeneous magnetic configuration in the NiFe layer cannot account for the measured reflectivities. One needs to consider that a small magnetisation rotation occurs inside the NiFe layer with respect to the CoFe layer (see Fig. 8d). This small rotation of the NiFe layer, almost non visible in the magnetisation curve, is clearly revealed by the neutron reflectometry curves. Even at 8 mT, the free layer appears to be not fully aligned with the external magnetic field. This effect appears clearly on the SQUID measurements under 6 mT, (points A and C on Fig. 8b) but after A and C a small rotation still exists which is not detectable by SQUID measurements. The effect of that rotation is to induce a coherent rotation of the magnetic free layer, beginning from the bottom (Ta layer) to the top (CoFe layer) during the reversal. This effect avoids any domain formation and therefore leads to low frequency magnetic noise in the sensitive region of the GMR. The maximal angle of rotation of the magnetisation in NiFe is fixed by a competition between the anisotropy and the exchange. This gives a rotation of about 5°/nm (as in NiFe domain walls) and then about 25° for the total NiFe layer in reasonable agreement with the maximum rotation observed in the layer ($30 \pm 5°$). This example illustrates a precise determination of the magnetic configuration using PNR. Very small rotations of magnetic moments in a specific layer can be determined allowing an in depth understanding of the magnetic evolution of the system under an applied field.

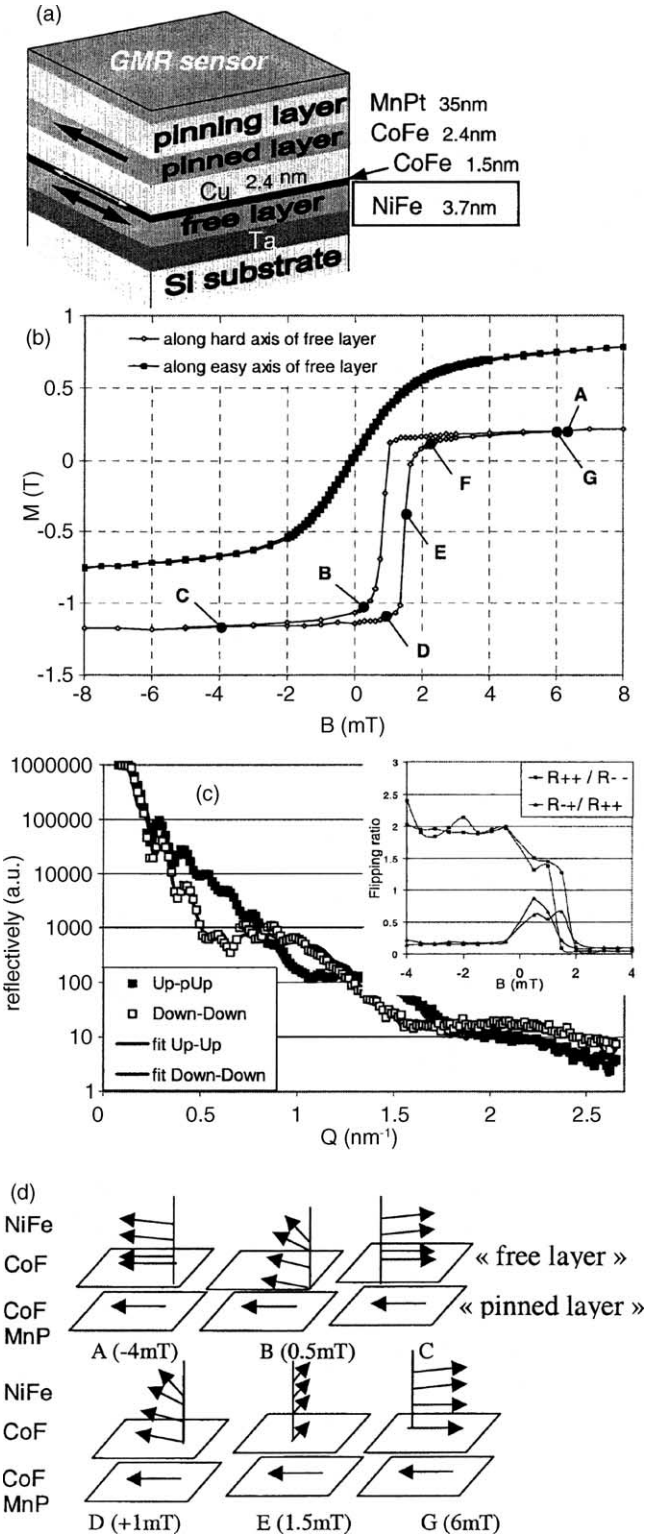

Fig. 8. Polarised neutron magnetometry on a GMR system: (a) a typical GMR structure; (b) SQUID measurement on the system. The (○) curve has been shifted vertically by −0.5 T for clarity. In such low magnetic fields, only the magnetisation of the "free" layer is modified. The observed magnetisation curves are driven by the magnetic coupling of the "free" layer with the pinned layer through the Cu spacer. This coupling is responsible for the horizontal shift of the (○) hysteresis curve. In the other direction (●), perpendicular to the magnetisation of the pinned layer, the coupling does not induce a shift but only an anisotropy. On top of this phenomenon (which is the basis of the operation of a spin-valve), during the fabrication, an "intrinsic" anisotropy, perpendicular to the "pinned" layer direction is induced in the "free" layer. This is done to prevent the formation of magnetic domains; (c) PNR on the GMR system measured in a planar field of 1 T along the "pinned" layer magnetisation, (inset) variation of the PNR signal as a function of the applied field measured at a fixed $\mathbf{Q} = 0.25\,\mathrm{nm}^{-1}$; (d) magnetic configuration of the different magnetic layers in the GMR system as a function of the field as deduced from the PNR measurement.

6. Useful resources

The technique of neutron reflectivity is now well established across Europe and a large wealth of literature is available. A large number of neutron reflectometers is now available across Europe: at the ILL (D17, ADAM), at the LLB (EROS, PRISM), at ISIS (CRISP, SURF), at Jülich (HADAS), at HMI (V6), soon at Munich FRMII (REFSANS). A list of all the existing neutron reflectometers can be found at [14]. You can apply usually twice a year to these facilities to perform your experiments. The web sites [56,57] gives you links to neutron reflectivity simulation and fitting programs. If you are interested in "industrial" application of neutron scattering, you may refer to the following web links [58].

7. Conclusion

Neutron reflectometry offers several specificities which makes it very useful for the study of polymer and magnetic thin film systems. In the field of soft matter, the possibility of deuteration and selective labelling makes neutron reflectivity an invaluable tool. In the field of magnetic thin films, the main advantages are that it is a direct probe of the magnetisation in a material. It can easily be used to measure AFM, ferro or helical ordering in super-lattices, probe complex magnetic ordering in multilayers, give detailed insights in problems such as the magnetism of ultra-thin film or the bias exchange mechanism. The limitations are that PNR is not element specific and that the neutron fluxes are still low. This last limitation could be removed when new neutron spallation sources will come into operation in the next 5–10 years.

References

[1] G.P. Felcher, R.O. Hilleke, R.K. Crawford, J. Haumann, R. Kleb, G. Ostrowski, Rev. Sci. Instrum. 58 (1987) 609–619.
[2] C.F. Majkrzak, J.W. Cable, J. Kwo, M. Hong, D.B. McWhan, Y. Yafet, J. Waszcak, Phys. Rev. Lett. 56 (1986) 2700–2703.
[3] J. Penfold, R.K. Thomas, J. Phys. Condens. Matter. 2 (1990) 1369–1412.
[4] T.P. Russel, Mat. Sci. Rep. 5 (1990) 171–271;
T.P. Russel, Physica B 221 (1996) 267–283.
[5] L.T. Lee, D. Langevin, B. Farnoux, Phys. Rev. Lett. 67 (1991) 2678–2681.
[6] J. Penfold, E.M. Lee, R.K. Thomas, Mol. Phys. 68 (1989) 33–47.
[7] M.N. Baibich, J.M. Broto, A. Fert, F. Nguyen-Van-Dau, F. Petroff, P. Etienne, G. Creuzet, A. Friederich, J. Chazelas, Phys. Rev. Lett. 61 (1988) 2472–2475.
[8] J. Lekner, Theory of Reflection of Electromagnetic and Particle Waves, Martinus Nijhoff, Dordrecht, 1987.
[9] C. Fermon, F. Ott, A. Menelle, Neutron reflectivity, pp. 163;
F. de Bergevin, Neutron reflectivity, in: J. Daillant, A. Gibaud (Eds.), X-ray, Neutron Reflectivity: Principles and Applications, Springer Lecture Notes in Physics, Berlin, 1999, pp. 3.
[10] V.F. Sears, Phys. Rep. 141 (1986) 281.
[11] V.F. Sears, Methods of Experimental Physics, vol. 23A, Neutron Scattering, Academic Press, Orlando, 1987;
V.F. Sears, Neutron News, vol. 3, 1992.
[12] http://www.neutron.anl.gov.
[13] G.P. Felcher, Physica B 267–268 (1999) 154–161.
[14] A list of all existing neutron reflectometers can be found at: http://www.studsvik.uu.se/research/NR/reflect.htm.
[15] C.F. Majkrzak, Physica B 221 (1996) 342–356.
[16] T.P. Russel, A. Menelle, W.A. Hamilton, G.S. Smith, S.K. Satija, C.F. Majkrzak, Macromolecules 24 (1991) 5721–5726.
[17] X. Zhao, W. Zhao, X. Zheng, M.H. Rafailovich, J. Sokolov, S.A. Schwarz, M.A. Pudensi, T.P. Russell, S.K. Kumar, L.J. Fetters, Phys. Rev. Lett. 69 (1992) 776–779.
[18] L.T. Lee, O. Guiselin, A. Lapp, B. Farnoux, J. Penfold, Phys. Rev. Lett. 67 (1991) 2838–2841.
[19] O. Guiselin, L.T. Lee, B. Farnoux, A. Lapp, J. Chem. Phys. 95 (1991) 4632–4640.
[20] L.T. Lee, B. Jean, A. Menelle, Langmuir 15 (1999) 3267–3272.
[21] C. Marzolin, P. Auroy, M. Deruelle, J.-P. Folkers, L. Leger, A. Menelle, Macromolecules 34 (25) (2001) 8694–8700.
[22] M. Geoghegan, F. Boue, G. Bacri, A. Menelle, D.G. Bucknall, Eur. Phys. J. B 3 (1998) 83–96.
[23] M. Lbsche, J. Schmitt, G. Decher, W.G. Bouwman, K. Kjaer, Macromolecules 31 (1998) 8893.
[24] B. Cathala, F. Cousin, http://www-llb.cea.fr/activ01–02/p122–123.pdf.
[25] C. Devaux, E. Beyou, Ph. Chaumont, J.P. Chapel, Eur. Phys. J. E: Soft Matter E 7 (2002) 345–352;
C. Devaux, J.P. Chapel, Eur. Phys. J. E: Soft Matter 10 (2003) 77–81.
[26] O. Prucker, J. Rühe, Macromolecules 31 (1998) 592.
[27] V. Bertagna, A. Menelle, S. Petitdidier, D. Levy, M.-L. Saboungi, in: R.E. Sah, M.J. Deen, D. Landheer, K.B. Sundaram, W.D. Brown, D. Misra (Eds.), Proceedings of the International Symposium on Silicon Nitride and Silicon Dioxide Thin Insulating Films VII, vol. 2, 2003, pp. 525–532.
[28] H. Chen-Mayer, G.P. Lamaze, S.K. Satija, AIP Conf. Proc. 550 (2001) 407–411.
[29] G. Battaglin, A. Menelle, M. Montecchi, E. Nichelatti, P. Polato, Glass Technol. 43 (5) (2002) 203–208.
[30] G. Fragneto-Cusani, J. Phys.: Condens. Matter 13 (2001) 4973–4989.
[31] D.E Bürgler, P. Grünberg, S.O. Demokritov, M.T. Johnson, Interlayer exchange coupling in layered magnetic structures, in: K.H.J Buschow (Ed.), Handbook of Magnetic Materials, vol. 13, Elsevier, Amsterdam, 2001, p. 1.
[32] A. Schreyer, C.F. Majkrzak, T. Zeidler, T. Schmitte, P. Bodeker, K. Theis-Brohl, A. Abromeit, J. Dura, T. Watanabe, Phys. Rev. Lett. 79 (1997) 4914–4917.
[33] J. Noguès, I.K. Schuller, J. Magn. Magn. Mater. 192 (1999) 203–232.
[34] M.R. Fitzsimmons, P. Yashar, C. Leighton, I.K. Schuller, J. Nogues, C.F. Majkrzak, J.A. Dura, Phys. Rev. Lett. 84 (2000) 3986–3989.
[35] C. Leighton, M.R. Fitzsimmons, A. Hoffmann, J. Dura, C.F. Majkrzak, M.S. Lund, I.K. Schuller, Phys. Rev. B 65 (2002) 064403/1–064403/7.
[36] F. Radu, M. Etzkorn, T. Schmitte, R. Siebrecht, A. Schreyer, K. Westerholt, H. Zabel, J. Magn. Magn. Mater. 240 (2002) 251–253.
[37] M. Gierlings, M.J. Prandolini, H. Fritzsche, M. Gruyters, D. Riegel, Phys. Rev. B 65 (2002) 092407/1–092407/4.
[38] S.G.E. te Velthuis, A. Berger, G.P. Felcher, B.K. Hill, E. Dan Dahlberg, J. Appl. Phys. 87 (2000) 5046.
[39] S.G.E. te Velthuis, G.P. Felcher, S. Jiang, A. Inomata, C.S. Nelson, A. Berger, S.D. Bader, Appl. Phys. Lett. 75 (1999) 4174–4176.
[40] D. Haskel, G. Srajer, J.C. Lang, J. Pollmann, C.S. Nelson, J.S. Jiang, S.D. Bader, Phys. Rev. Lett. 87 (2001) 207201/1–207201/4.
[41] K.V. O'Donovan, J.A. Borchers, C.F. Majkrzak, O. Hellwig, E.E. Fullerton, Phys. Rev. Lett. 88 (2002) 067201/1–067201/4.

[42] E.E. Fullerton, S.D. Bader, J.L. Robertson, Phys. Rev. Lett. 77 (1996) 1382–1385.
[43] P. Bodeker, A. Schreyer, H. Zabel, Phys. Rev. B 59 (1999) 9408–9431.
[44] V. Leiner, D. Labergerie, R. Siebrecht, Ch. Sutter, H. Zabel, Physica B 283 (2000) 167–170.
[45] S.J. Blundell, J.A.C. Bland, Phys. Rev. B 46 (1992) 3391–3400.
[46] C. Fermon, C. Miramond, F. Ott, G. Saux, J. Neutron Res. 4 (1996) 251.
[47] Z. Pleshanov, Physica B 94 (1994) 233–243.
[48] H. Zabel, R. Siebrecht, A. Schreyer, Physica B 276–278 (2000) 17–21.
[49] H. Zabel, K. Theis-Brohl, J. Phys.: Condens. Matter 15 (2003) S505–S517.
[50] G.P. Felcher, J. Appl. Phys. 87 (2000) 5431–5436.
[51] Y.Y. Huang, G.P. Felcher, S.S.P. Parkin, J. Mag. Mag. Mater. 99 (1991) 31–38.
[52] A. Schreyer, J.F. Aukner, T. Zeidler, H. Zabel, C.F. Majkrzak, M. Schaefer, P. Gruenberg, Euro. Phys. Lett. 32 (1995) 595–600.
[53] W. Szuszkiewicz, K. Fronc, M. Baran, R. Szymczak, F. Ott, B. Hennion, E. Dynowska, W. Paszkowicz, J. Pelka, R. Zuberek, M. Jouanne, J.F. Morhange, J. Supercond.: Incorporat. Novel Magn. 16 (2003) 205–208.
[54] W. Szuszkiewicz, E. Dynowska, F. Ott, B. Hennion, M. Jouanne, J.F. Morhange, J. Sadowski, J. Supercond.: Incorporat. Novel Magn. 16 (2003) 209–212.
[55] H. Kepa, J. Kutner-Pielaszek, A. Twardowski, C.F. Majkrzak, J. Sadowski, T. Story, T.M. Giebultowicz, Phys. Rev. B 64 (2001) 121302/1–121302/4. R.
[56] http://www-llb.cea.fr/prism/PRISM.html.
[57] http://www.neutron.anl.gov/software.html.
[58] Links towards possible industrial applications of neutron scattering: http://www-llb.cea.fr/industrie/index.html or http://www.ill.fr/index_ind.html.